Open Archive Toulouse Archive Ouverte

OATAO is an open access repository that collects the work of Toulouse researchers and makes it freely available over the web where possible

This is an author's version published in: http://oatao.univ-toulouse.fr/20437

Impedance analysis of film-forming amines for the corrosion protection of a carbon steel

Jordan Baux [a, b], Nicolas Caussé [a], Jérôme Esvan [a], Sophie Delaunay [b], Jonathan Tireau [b], Marion Roy [c], Dominique You [c], Nadine Pébère [a, *]

[a] *Université de Toulouse, CIRIMAT, UPS/INPT/CNRS ENSIACET, 4 allée Emile Monso, 31030, Toulouse Cedex 4, France*
[b] *EDF R&D / MMC / Chemistry and Corrosion Group, Avenue des Renardières, 77818, Moret-sur-Loing Cedex, France*
[c] *DEN — Service d'Etude du Comportement des Radionucléides (SECR), CEA, Université Paris-Saclay, 91191, Gif-sur-Yvette, France*

A B S T R A C T

Octadecylamine (ODA) is a well-known organic inhibitor for the corrosion protection of carbon steels. In the present study, electrochemical impedance data analysis was performed to extract physical parameters of the ODA thin film that formed on a P275 carbon steel surface. First, surface observations and contact angle measurements showed the steel surface modification after the ODA treatment linked to the adsorption of an organic hydrophobic thin film. X-ray photoelectron spectroscopy confirmed the presence of a very thin organic layer and revealed the presence of iron oxide/hydroxide underlying the ODA film. The impedance data analysis with a power-law distribution of resistivity in the organic film allowed the permittivity and thickness to be extracted. Finally, from the impedance results with and without ODA, the instantaneous corrosion inhibition efficiency was determined.

1. Introduction

During shutdown periods of pressurized water reactors (PWR) for maintenance operation, strict and restrictive conservation conditions must be respected in order to preserve the secondary circuit of any oxidation phenomenon. Use of inhibitors, such as film-forming amines (FFA), is a promising approach to simplify the conservation conditions while reducing or stopping the corrosion of carbon steel, which constitutes the major part of the PWR secondary circuit [1,2]. A key benefit of FFA is to improve the corrosion protection during start-ups and shutdowns of the PWR and, as a consequence, high steam quality can be obtained quicker during start-up, leading to significant economic benefits [1]. Even though FFA have been used successfully for decades to treat water in industrial power plants [3], its behaviour is not well understood as well as the physical characteristics of the film formed on the carbon steel surface. Octadecylamine (ODA), $CH_3(CH_2)_{17}NH_2$, one of the simplest FFA molecule, has been used for steel protection in nuclear power and fossil fuel power plants for many years [1,3−12]. The molecule has both a hydrophilic head and a hydrophobic tail, which after the film formation creates a physical barrier that impedes water, oxygen or other corrosive agents to reach the metal surface and also probably prevents iron dissolution (anodic and cathodic effects). The protective film is often described as a monolayer formed on the steel surface [2,10,13,14] but proof of its thickness has never been provided. The determination of the film thickness would be of great interest to better control the ODA injection in the secondary circuit. However, *in situ* determination of organic ultra-thin films thickness remains quite challenging, moreover on rough surfaces [15−18]. Mechanical and optical profilometry are not sensitive enough to investigate the film thickness at a sub-micrometric scale. Other optical techniques, such as ellipsometry, require the knowledge of physical quantities (refractive index, for example) and the use of modelling to extract the film thickness from the experimental data [18]. Atomic force microscopy (AFM) can be used for *in situ* determination of very thin film thickness but the measurements are strongly sensitive to the substrate roughness. For an ODA film deposited on mica, Patil et al. have measured, by AFM and in humid conditions, a thickness of about 20−30 nm [18]. On the other hand, x-ray photoelectron spectroscopy (XPS) and secondary ion-mass spectroscopy (SIMS) are powerful *ex situ* techniques that allow surface characterization and thickness

measurement at a nanometric scale. However, the erosion rate, which depends on the material, must be known for an accurate thickness determination.

Electrochemical impedance spectroscopy (EIS) is a widely used technique for the assessment of the corrosion protection by inhibitors and coatings. This technique allows *in situ* measurements in controlled experimental conditions, which can be representative of real environment [19–22]. Recently, good agreement has been found between results obtained from EIS data and XPS analysis for the determination of a thin oxide layer thickness [23–28].

The aim of the present work was to determine the thickness of an ODA film formed on a carbon steel surface at 80 °C in an alkaline solution. These pH and temperature conditions are close to that encountered in the PWR secondary circuit. First, the film formed on the carbon steel electrode was characterized by *ex situ* observations and XPS analysis. Then, the impedance diagrams obtained in the solution in the presence of ODA was compared with a model to determine the thickness and the dielectric permittivity of the organic film. From the impedance diagrams obtained at the corrosion potential, with and without ODA, the instantaneous corrosion inhibition efficiency was assessed.

2. Experimental

2.1. Materials

The P275 low carbon steel was supplied by EDF (France) as representative material of the PWR. Its composition is reported in Table 1. The steel sample was machined to obtain a cylindrical rod of 1.13 cm in diameter (surface area = 1 cm^2). The lateral part of the rod was covered with a heat-shrinkable insulating sheath, leaving only the tip of the carbon steel in contact with the solution. The steel surface was wet ground with silicon carbide (SiC) papers down to grade 4000, ultrasonically cleaned with ethanol, rinsed with deionized water and dried.

The chosen FFA was octadecylamine (ODA) in the form of ODACON®, a commercial emulsion (≈ 50 g/L FFA) supplied by REICON™.

The electrolyte solution was prepared from deionized water by adding Na_2SO_4 10^{-3} M (analytical grade). The pH of the solution was adjusted at 10 with ammonia (99.99%). The choice of this medium was based upon its low electrical conductivity, close to that encountered in industrial water circuits, its low corrosiveness toward carbon steel and because it is an easily reproducible baseline solution. The same solution was used for the film formation and for the electrochemical impedance measurements.

2.2. Film formation

The optimum conditions (ODA concentration, temperature, pH of the solution, immersion time and electrode rotation rate) to achieve a homogeneous film formation were determined from preliminary experiments. In the present work, the chosen experimental conditions are reported in Table 2. With these parameters, a protective ODA film was formed on the carbon steel surface in less than 30 min.

For the surface analysis (optical observations, contact angle measurements and XPS), the samples were removed from the

Table 1
Chemical composition (wt. %) of the P275 carbon steel (EN10028-3).

Element	C	Si	Mn	Cr	Mo	Ni	Cu	Fe
	0.16	0.4	0.5–1.5	0.3	0.08	0.5	0.3	Bal.

Table 2
Parameters for the formation of the ODA film.

ODA concentration	100 mg kg^{-1}
Temperature	80 °C
Electrode rotation rate	500 rpm
pH$_{25°C}$	10
Immersion time	30 min

electrolytic solution and kept in contact with air. For the electrochemical measurements, after the film formation according to the conditions reported in Table 2, the cell was left at room temperature and all the parameters were kept constant. The diagrams were obtained after 2 h of immersion in the same electrolyte. The sample after the film formation is henceforth called the ODA treated sample.

2.3. Surface characterizations

Optical observations were performed with a binocular and an Olympus PMG3 optical microscope. The contact angles were measured at room temperature using a Digidrop Contact Angle Meter from GBX Scientific Instruments. The protocol consisted in depositing a deionized water drop of an accurate volume of 2 μL on the sample surface (bare carbon steel surface or ODA treated sample) and then measuring the static contact angle, 60 s after the drop deposition. To assess the homogeneity of the surface properties, 20 measurements were performed on different locations over the samples surface.

The chemical composition of the film formed on the carbon steel surface was determined using XPS analysis carried out on a K alpha Thermo Scientific Spectrometer. The specimens were irradiated with a Al-Kα radiation (hυ = 1486.6 eV) from a monochromatized source and the x-ray spot was approximately 400 μm in size. Angle-resolved measurements were made at a take-off angle θ = 90° (e.g. normal to the sample surface). For the surveys spectra, pass energy was fixed at 160 eV and at 40 eV for high resolution spectra. The energy calibration was made using the Au 4f 7/2 (83.9 ± 0.1 eV) and Cu 2p 3/2 (932.8 ± 0.1 eV) photoelectron lines. XPS spectra were recorded in direct N(Ec). Background signal was removed using Shirley method. The binding energy scale was established by referencing the C 1s value of adventitious carbon (284.9 ± 0.1 eV). The photoelectron peaks were analysed by Gaussian/Lorentzian (G/L = 30) peak fitting. Flood gun was also applied for avoiding charge effects. The analyses were performed on two ODA treated samples and at various locations to verify the homogeneity of the layer.

2.4. Electrochemical measurements

The electrochemical measurements were performed with a conventional three-electrode cell with a saturated sulphate reference electrode and a platinum grid, as counter electrode. The working electrode consisted of the carbon steel rod. The rotation rate was fixed at 500 rpm. Electrochemical impedance measurements were performed using a Solartron 1286 electrochemical interface connected to a Solartron 1250 frequency response analyser. Impedance diagrams were obtained under potentiostatic regulation at the corrosion potential (E_{corr}) in the frequency range of 65 kHz to 10 mHz with 8 points per decade, using a 15 mV$_{rms}$ sinusoidal voltage. Impedance data beyond 6.5 kHz were not taken into account due to experimental artefacts [29]. The obtained impedance diagrams were always consistent with the Kramers-Kronig relations [30–32]. Data modelling was carried out with a non-commercial software developed at the LISE CNRS (Paris).

3. Impedance diagrams analysis

The impedance results for the ODA treated sample were analysed in two successive steps in order to determine the organic film thickness. The first approach was based on graphical methods, independent of any physical model [23,33,34]. The second approach was focused on the use of the power-law resistivity model developed by Hirschorn et al. [35,36]. Both methodologies are briefly recalled in the following sections.

3.1. Graphical methods

The impedance results are commonly analysed by using electrical equivalent circuits (EEC). However, it is observed that resistances and capacitances, which are associated with different steps of the corrosion process, inhibitor or coating properties do not accurately describe the experimental impedance data. In these cases, constant phase elements (CPE) were used instead of capacitances to take into account the non-ideal behaviour of the system. The CPE impedance is expressed in terms of model parameters α and Q as:

$$Z_{CPE} = \frac{1}{(j\omega)^\alpha Q} \tag{1}$$

with $\omega = 2\pi f$. The α parameter can be extracted by plotting the logarithm of the imaginary part of the impedance (Z_j) with respect to the logarithm of the frequency (Eq. (2)) [33]. Q is expressed as a function of α and impedance data (Eq. (3)):

$$\alpha = \frac{dlog(-Z_j)}{dlog(f)} \tag{2}$$

$$Q = \sin\left(\frac{\alpha\pi}{2}\right)\frac{-1}{Z_j(f)(2\pi f)^\alpha} \tag{3}$$

In the case of a 3D dielectric layer on a conducting electrode surface, the CPE parameters can be directly related to the physical properties of the layer. For oxide films or organic coatings, the capacitance of the layers can be extracted from the impedance data by using the complex-capacitance representation [23–25,34,37].

$$C(\omega) = \frac{1}{j\omega[Z(\omega) - R_e]} \tag{4}$$

The value of the electrolyte resistance, R_e, must be accurately determined from extrapolation at high-frequency on the real axis of the Nyquist diagram to correctly represent the complex-capacitance plots. Once the capacitance of the layer, C_f, is known, the layer thickness, δ_f, can be calculated from the relationship:

$$\delta_f = \frac{\varepsilon\varepsilon_0}{C_f} \tag{5}$$

where ε is the permittivity of the film and ε_0, the permittivity of vacuum.

It is noteworthy that with an accurate estimate for the electrolyte resistance a modified Bode representation, corrected from the ohmic drop, can be obtained from the following relationships (Eq. (6) and Eq. (7)). This allows the CPE behaviour to be clearly observed in the high-frequency domain.

$$|Z| = \sqrt{(Z_r - R_e)^2 + (Z_j)^2} \tag{6}$$

$$\Phi = tan^{-1}\left(\frac{Z_j}{(Z_r - R_e)}\right) \tag{7}$$

where Z_r and Z_j are the real part and the imaginary part of the impedance.

3.2. Power-law resistivity model

Recently, different studies suggested that the origin of the CPE behaviour observed with oxide films or organic coatings may be the consequence of a normal distribution of their resistivity along the film thickness according to the model developed by Hirschorn et al. [35,36]. The resistivity $\rho(\xi)$, with $\xi = \frac{x}{\delta}$, is expressed (Eq. (8)) as a function of the layer thickness, δ, the depth, x, in the layer, the boundary resistivity values ρ_0 and ρ_δ at the metal/film interface ($x = 0$) and at the film/electrolyte interface ($x = \delta$) and γ which is derived from the CPE parameter α such as $\alpha = \frac{(\gamma-1)}{\gamma}$.

$$\frac{\rho(\xi)}{\rho_\delta} = \left(\frac{\rho_\delta}{\rho_0} + \left(1 - \frac{\rho_\delta}{\rho_0}\right)\xi^\gamma\right)^{-1} \tag{8}$$

The corresponding impedance can be determined by using an integral expression:

$$Z_f(\omega) = \delta \int_0^1 \frac{1}{\frac{1}{\rho_0} + j\omega\varepsilon\varepsilon_0 + \left(\frac{1}{\rho_\delta} - \frac{1}{\rho_0}\right)\xi^\gamma}d\xi \tag{9}$$

Regression of EIS data with the power-law model allows the extraction of physical parameters related to the film, such as the permittivity, the thickness and the resistivity values ρ_0 and ρ_δ at the interfaces which are not easily accessible by other techniques. According to Hirschorn et al. [35], for a frequency lower than $f_\delta = (2\pi\rho_\delta\varepsilon\varepsilon_0)^{-1}$, an analytical expression of the impedance of the film can be written as:

$$Z_f(\omega) = g\frac{\delta\rho_\delta^{1-\alpha}}{\left(\rho_0^{-1} + j\omega\varepsilon\varepsilon_0\right)^\alpha} \tag{10}$$

Where

$$g = 1 + 2.88(1 - \alpha)^{2.375} \tag{11}$$

This impedance shows a CPE behaviour in the high-frequency range ($f < f_\delta$) with α and Q as parameters and

$$Q = \frac{(\varepsilon\varepsilon_0)^\alpha}{g\delta\rho_\delta^{(1-\alpha)}} \tag{12}$$

with ρ_δ, the resistivity at the film/electrolyte interface as discussed above.

The resistivity at the metal/film interface ρ_0 can be calculated by using the characteristic frequency, f_0, graphically determined at the maximum of the imaginary part of the impedance:

$$\rho_0 = \frac{1}{2\pi\varepsilon\varepsilon_0 f_0} \tag{13}$$

4. Results and discussion

4.1. Morphology and hydrophobicity of the samples surface

Fig. 1 shows the carbon steel surface after 30 min in the electrolyte at 80 °C with and without ODA. Without ODA, corrosion products with the shape of hydrodynamic pattern are observed (Fig. 1a). Similar photographs, taken *in situ*, for the corrosion of pure iron in neutral chloride solutions, have shown that with increasing immersion time (24 h), the corrosion led to the formation of porous layers which progressively decreased the active area of the bare metal [38]. In the presence of ODA, 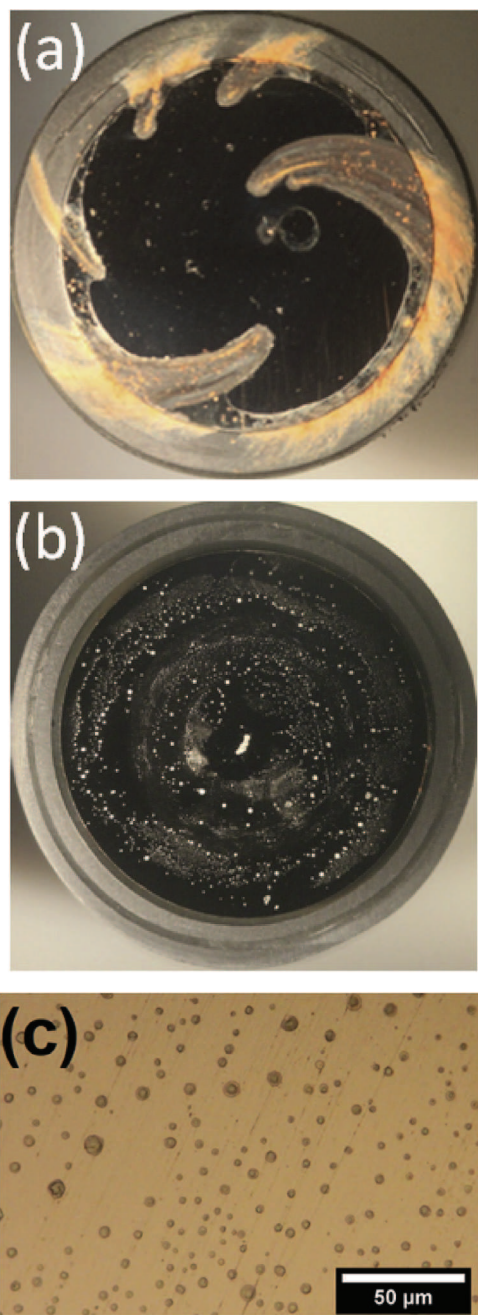the carbon steel surface is not attacked but covered with scattered small round clusters (Fig. 1b). Their dimensions ranged from 0.1 to 5 μm (Fig. 1c). Raman spectroscopy analysis (results not shown) have revealed that the clusters are made of bulk ODA. From these photographs, it can be assumed that ODA molecules covered the entire carbon steel surface.

Contact angle measurements were performed on the bare carbon steel surface and on the ODA treated sample. The results are shown in Fig. 2. For the bare steel, the surface presented a hydrophilic character with a contact angle value of 39° ± 5° (Fig. 2a). For the ODA treated sample (Fig. 2b), the contact angle value is 93° ± 2° showing that the surface lost its hydrophilic character, which is a well-known effect of the ODA adsorption [1]. The weak variation of the contact angle for the ODA treated sample (Fig. 2b) indicates that the hydrophobic film is homogeneous even in the presence of ODA aggregates on the surface.

4.2. XPS analysis

Fig. 3 shows the surveys spectra for the bare carbon steel surface (Fig. 3a) and for the ODA treated sample (Fig. 3b). On Fig. 3b, independently of the sample and of the analysed area, the spectra are superimposed and Fe, O, C and N peaks are observed confirming a homogeneous coverage of the carbon steel surface by the ODA molecules. The N signal is not observed in Fig. 3a, and in contrast, in Fig. 3b, the small N peak and the intense C peak are associated to the presence of the ODA molecules. Fig. 4 displays the high resolution spectra of N 1s, C 1s, Fe 2p3/2 and O 1s. The binding energies for the different signals are summarised in Table 3 as well as the chemical composition of the surface (in at. %), calculated from the peak area.

The N 1s spectrum exhibits two peaks at 399.5 eV and 401.1 eV which can be assigned to the NH_2 [39–42] and NH^{3+} [17,43,44] groups, respectively. The binding energy difference between NH_2 and NH^{3+} (1.6 eV) is in agreement with previous studies [43,44]. The same binding energy has been reported for NH_2 in the case of Pd and Ag substrates: CH_3NH_2/Pd [39], $CH_3CH_2NH_2$/Ag [40],

Fig. 1. Optical observations of the carbon steel surface after immersion in the electrolyte at 80 °C, $pH_{25\,°C} = 10$, $\Omega = 500$ rpm during 30 min: (a) without ODA, (b) with ODA (surface area: 1 cm²) and (c) zoom of the ODA treated sample surface.
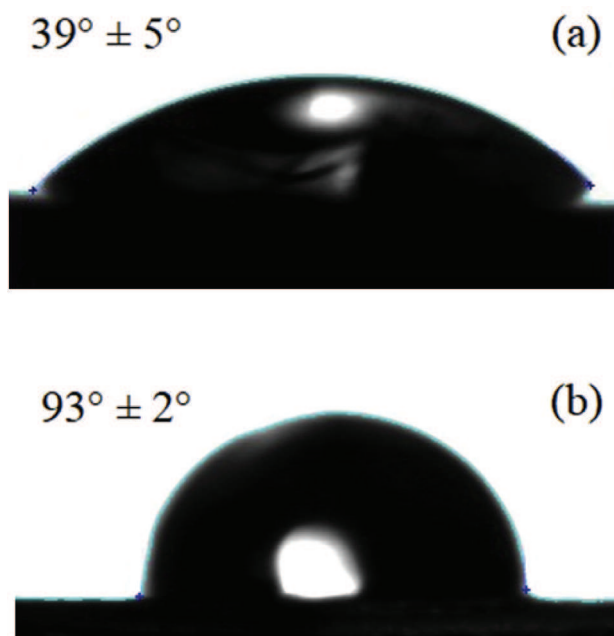

Fig. 2. Contact angles measured on: (a) the bare carbon steel and (b) the treated ODA sample.
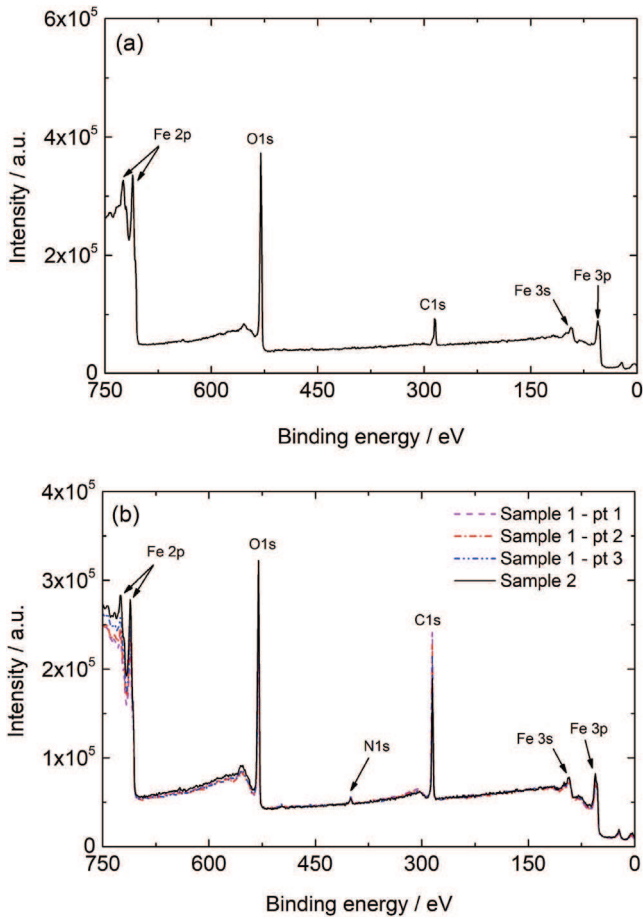
Fig. 3. XPS survey spectra of: (a) the bare steel surface and (b) the ODA treated sample surface. In Fig. 3b, the spectra were obtained for two samples and on different locations.

Table 3
Chemical composition of the treated ODA steel surface obtained from XPS analysis.

Components	Binding Energy (eV)	FWHM[a] (eV)	At. %
C 1s (C—C, C—H)	285.0	1.1	47
C 1s (C—N/C—O)	286.1	1.6	3.7
C 1s (O—C=O)	288.3	1.5	1.6
O 1s (O^{2-} (iron oxide))	529.7	1.2	20.8
O 1s (OH^- (iron hydroxide))	531.5	1.5	10.1
O 1s (pollution)	532.4	1.9	1.6
N 1s (NH_2)	399.5	1.6	1.6
N 1s (NH^{3+})	401.1	2	0.4
Fe 2p3/2 (metal)	706.3	1.8	5.6
Fe 2p3/2 (oxide)	708.0	—	7.6
Total			100
N/C ratio			0.042

[a] Full width at half maximum.

$NH_2(C_6H_4)O(C_6H_4)NH_2$/Ag [41] and ODA on graphene oxide substrate [42]. The C 1s spectrum displayed three peaks: the first one at 285 eV can be ascribed to the aliphatic C—C bond of the ODA molecule [42]. The second one at 286.1 eV is attributed to C—O and C—N bonds. The third, small peak at 288.3 eV is characteristic of C—N bonds in amides or O=C—O bonds [42] which would be due to surface pollution. For the Fe 2p spectrum, a first peak appears at 706.3 eV due to metallic iron and a second peak, beyond 710 eV, relates to iron oxides [45]. The O 1s spectrum is composed of at least two peaks: one at 529.7 eV relates to O^{2-} (iron oxides) [44], and a second one at 531.5 eV attributed to the OH^- ions [46]. A small peak at 532.4 eV would be linked to the surface pollution.
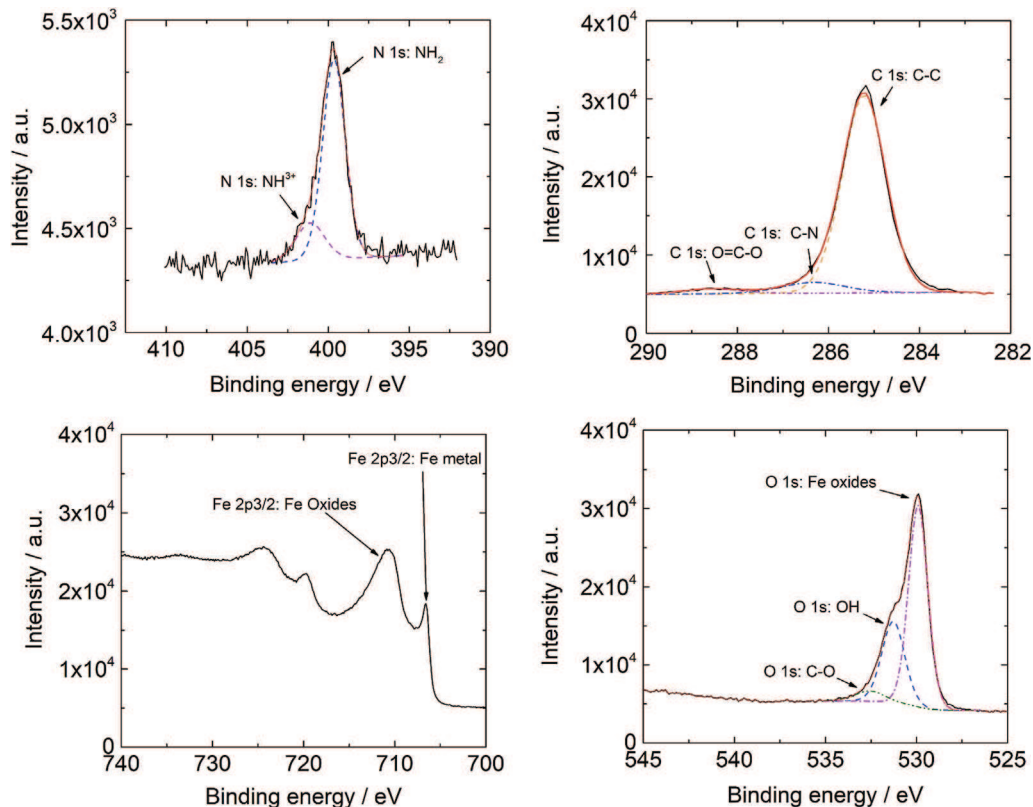

Fig. 4. High resolution XPS spectra of N 1s, C 1s, Fe 2p3/2 and O 1s for the ODA treated sample surface.

Thus, ODA might be adsorbed on a thin iron oxide/hydroxide layer, probably Fe_2O_3 or FeOOH and not directly on the bare carbon steel surface. The expected theoretical value for the $\frac{[N\ 1s]}{[C-C]}$ ratio in the ODA molecule is 0.055. A smaller value of 0.042 was calculated from the data reported in Table 3. This difference might be due to the surface pollution which increased the C−C contribution.

From the XPS analysis, both the signal from the organic molecules and from the substrate were observed. This indicated that the organic film thickness ranged from 2 nm (thickness of an ODA monolayer) to about 10 nm. This limit value was estimated from the short inelastic mean free path, λ, of electrons in condensed materials (about 3 nm). The major part of the signal is contained in a depth of 3λ [47], and therefore cannot exceed 10 nm. It must be also mentioned that a spontaneous film thickness reduction, known as "ripening" occurs when ODA self-assembled layers are in contact with air [18,43,44]. Besides, weakly adsorbed multilayers in the electrolyte may be damaged during the electrode removal from the solution [16].

4.3. EIS measurements

4.3.1. Graphical method analysis

Impedance spectra for the bare carbon steel and the ODA treated sample are presented in Fig. 5. The Nyquist diagrams (Fig. 5a) show depressed capacitive loops. For the non-treated sample, only one loop is observed. On the Bode plot (Fig. 5c), the symmetrical shape of the diagram did not indicate the presence of additional time-constants. For the ODA treated sample, the first loop at high-frequency, between 10^4 and 10^1 Hz, characterizes the organic film. This time constant is only visible on the phase angle in the presence of ODA (Fig. 5c). The second capacitive loop, between 10^1 and 10^{-2} Hz, can be attributed to the processes occurring at the metal/film interface. It was checked that the second loop was little dependent of the electrode rotation rate (diagrams not shown) indicating that this time constant is not due to diffusion phenomena in the solution.

First, the impedance data analysis focussed on the high-frequency time constant obtained for the ODA treated sample. Fig. 6 displays the impedance diagram in Bode coordinates corrected from the electrolyte resistance. On the phase angle plot and at high-frequency, a plateau is observed, characteristic of a pure CPE behaviour. The phase angle value on the plateau is θ = 68°. Thus, the CPE parameter α_f, is equal to 68:90 = 0.75.

Fig. 7 presents the complex-capacitance plot corresponding to the curve presented in Fig. 6, obtained from Eq. (4). The extrapolation of the high-frequency data to the real axis does not allow an accurate determination of the capacitance. However, it is possible to estimate a film capacitance value (C_f) between 0.1 and $0.2\ \mu F\ cm^{-2}$. Then, the film thickness can be obtained from Eq. (5). The permittivity of the ODA film is not known. In the literature, permittivity values of self-assembled surfactants were reported and the values ranged from 2 to 3 [48−53]. A value of 2.7, found for bulk ODA [53], was used in Eq. (5) to calculate the film thickness. From the estimation of the film capacitance, the ODA film thickness varied from 12 to 22 nm.

As already mentioned, the high-frequency time constant revealed a non-ideal behaviour described by a CPE (Fig. 6). The CPE parameters (α_f and Q_f) were also graphically determined (Fig. 8). Fig. 8a shows that the absolute value of the slope is 0.75, in agreement with the α_f value determined from Fig. 6. In Fig. 8b, the horizontal asymptote provides the Q_f value ($4.14\ \mu F\ cm^{-2}\ s^{(\alpha-1)}$). It was assumed that the CPE behaviour of the metal/ODA film/electrolyte interface was the result of a power-law dependence of the organic film resistivity; thus, the ρ_δ value can be framed by using Eq. (12) with the values of δ_f, Q_f and α_f graphically determined. The ρ_0
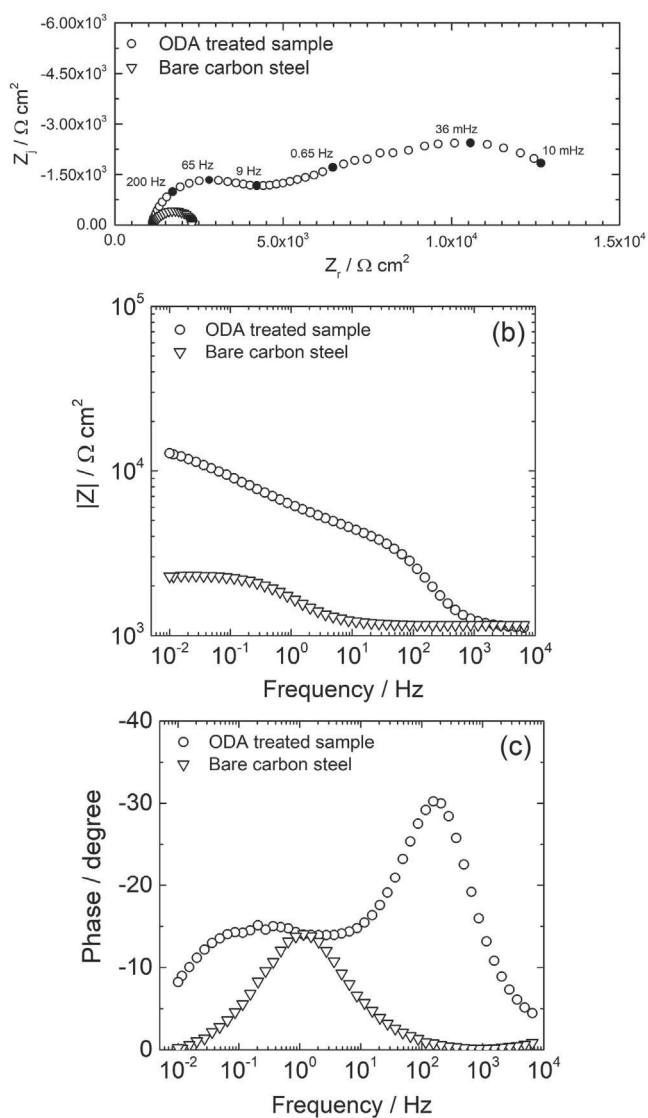

Fig. 5. Electrochemical impedance diagrams obtained at E_{corr} for the bare carbon steel and for the ODA treated sample after 2 h of immersion in the electrolyte: (a) Nyquist plot and (b) impedance modulus and (c) phase angle.
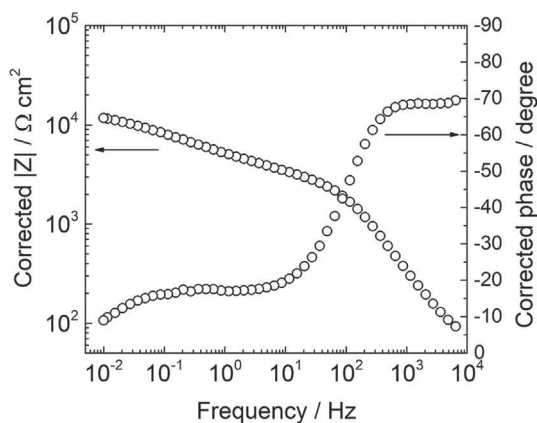

Fig. 6. Impedance diagram in Bode coordinates corrected from the ohmic resistance ($R_e = 1080\ \Omega\ cm^2$) for the ODA treated sample after 2 h of immersion in the electrolyte.
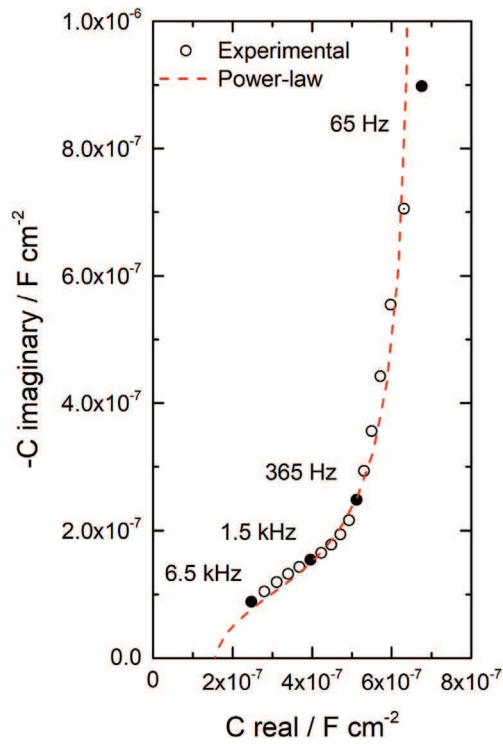
Fig. 7. Complex-capacitance plot corresponding to the EIS spectrum presented in Fig. 6. The dotted line is the best fitted curve according to Eq. (9).
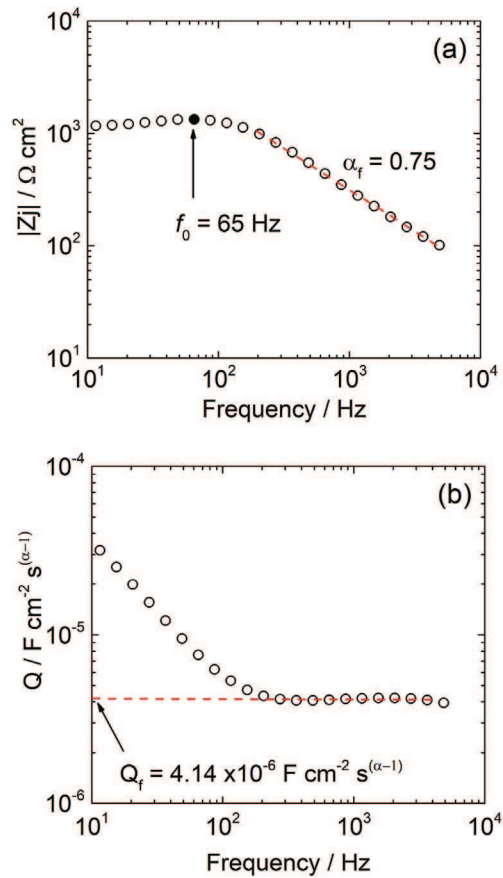

Fig. 8. (a) Logarithm of the imaginary part of the impedance vs. the logarithm of the frequency and (b) Q as a function of the frequency with $\alpha_f = 0.75$. High-frequency part of the diagram for the ODA treated sample.

value can be calculated using Eq. (13) with the value of $f_0 = 65$ Hz (f_0 is the characteristic frequency at the maximum of the imaginary part of the impedance determined in Fig. 8a). All the graphically determined parameters were reported in Table 4.

4.3.2. Impedance analysis with the power-law model

The high-frequency part of the diagram (6.5 kHz−65 Hz) was regressed from the integral expression of the power-law model (Eq. (9)). The best fitted curve is shown as dotted line in Fig. 7. A good fitting was achieved with a general sum of the deviations between experimental and calculated spectra $\chi^2 = 0.36$. The regression procedure provided numerical values of the adjustable parameters (α_f, ρ_0, ρ_δ, ε_f and δ_f) relevant to the ODA film. These values were reported in Table 4 for comparison with the graphically extracted parameters. A good agreement is obtained between the two procedures (Table 4). The film thickness obtained from the power-law model was equal to 16 nm and the permittivity value was close to the one found in the literature [53]. The values of ρ_0, ρ_δ and α_f were used to calculate the in-depth profile of the steel/ODA film/electrolyte interface (Eq. (8)). The result is shown in Fig. 9. A high resistivity area ($\rho_0 = 1 \times 10^{10}\,\Omega$ cm) is observed in a region close to the metal/film interface. This 2 nm thick layer might correspond to a close-packed ODA monolayer, considering a tilt angle of the ODA aliphatic chains of roughly 15° [43]. Beyond the 2 nm layer, the resistivity decreases to reach a minimum value of $1.6 \times 10^6\,\Omega$ cm at the film/electrolyte interface. These results would indicate a strong interaction between the first ODA layer in contact with the carbon steel surface (or the iron oxide/hydroxide layer). The additional layers would be less compact due to weaker interactions.

4.3.3. Corrosion inhibition efficiency

The ODA film formed on the carbon steel surface was assumed to be strongly adsorbed due to the high resistivity at the carbon steel/ODA film interface (Fig. 9). However, the low impedance values obtained after treatment would be indicative of the presence of porosities in the organic film (through pores). The corrosion process would occur on a reduced surface area. Thus, the second time constant on the impedance diagram for the ODA treated sample can be attributed to the charge transfer process at the bottom of the pores. The impedance diagram for the bare carbon steel and the low-frequency part of the diagram for the ODA treated sample were analysed and discussed below.

The parameters associated to the low-frequency capacitive loop, Q_{dl} and α_{dl}, as well as the electrolyte resistance, R_e, and the charge transfer resistance, R_t, for the bare carbon steel were graphically determined. For the ODA treated sample, the Q_{dl} and α_{dl} parameters could not be graphically determined due to the strongly depressed capacitive loop. An equivalent circuit (R//CPE) allowed an easier determination of the parameters associated with the low-frequency loop (Fig. 10). The R_e, R_t, Q_{dl}, and α_{dl} values are reported in Table 5. A value of $\alpha_{dl} = 0.44$ was obtained for the ODA treated sample. This value appeared abnormally weak and may be attributed to a porous electrode behaviour including the formation of pits at the bottom of the pores of the ODA film. Similar low values have been reported in the literature [54].

From the CPE parameters, the double layer capacitance (C_{dl}) value was calculated, considering a 2D distribution of the charge transfer resistances on the electrode surface, by using the Brug formula [55,56]:

$$C_{dl} = Q_{dl}^{\frac{1}{\alpha}}\left(\frac{1}{R_e} + \frac{1}{R_t}\right)^{(\alpha-1)/\alpha} \tag{14}$$

The C_{dl} values were 100 µF cm^{-2} and 12 µF cm^{-2} for the bare carbon steel and for the ODA treated sample, respectively. The

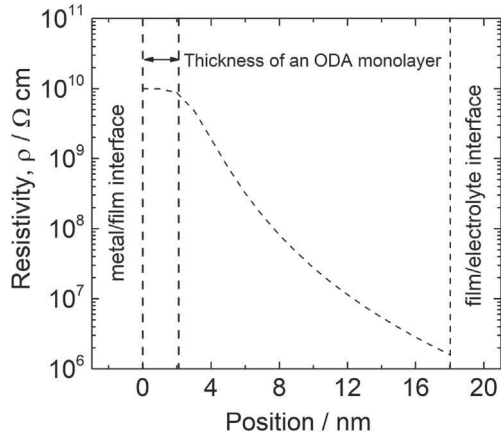|	ε	ρ_0 (Ω cm)	ρ_δ (Ω cm)	α_f	δ_f (nm)	R_e (Ω cm^2)
Graphically extracted values	2.7 [53]	1×10^{10}	$[1.5 \times 10^6; 2.4 \times 10^7]$	0.75	[12; 22]	1080
Regressed parameters	2.8	1×10^{10}	1.6×10^6	0.78	16	1080

Fig. 9. ODA film resistivity profile obtained from the impedance analysis (high-frequency part) as a function of position calculated from Eq. (8).
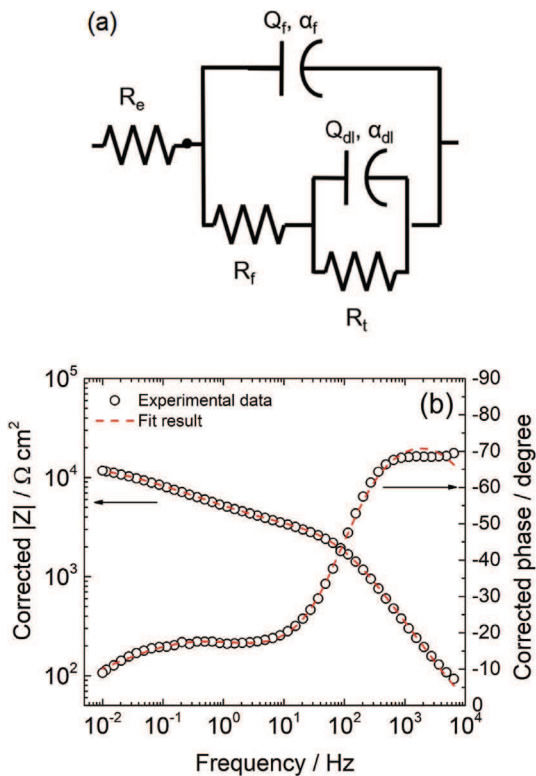

Fig. 10. (a) Electrical equivalent circuit used to fit the experimental diagram of the ODA treated sample and (b) electrochemical impedance diagram obtained at E_{corr} for the ODA treated sample. The experimental data are fitted with the equivalent circuit in Fig. 10a.

capacitance for the bare carbon steel is in the range of a double-layer capacitance ($\approx 50\,\mu$F cm^{-2}) [25].

The ratio of the capacitances for the bare carbon steel and the ODA treated sample gave an insight about the accessible surface

	R_e (Ω cm^2)	R_t (Ω cm^2)	Q_{dl} (F cm^{-2} s$^{(\alpha-1)}$)	α_{dl}	C_{dl} (μF cm^{-2})	IE (%)
Bare carbon steel	1157	1175	2.48×10^{-4}	0.68	100	–
Treated ODA sample	1080	11720	1.3×10^{-4}	0.44	12	90

area at the bottom of the through-pores of the ODA film. A value of 12% was obtained. The R_t values were used to calculate the instantaneous inhibitive efficiency (IE) according to the following equation:

$$IE\% = \frac{R_t^{inh} - R_t^0}{R_t^{inh}} \times 100 \qquad (15)$$

with $R_t^{inh} = 11720\,\Omega$ cm^2, the charge transfer resistance for the ODA treated sample and $R_t^0 = 1175\,\Omega$ cm^2, the charge transfer resistance for the bare carbon steel. The calculated IE was equal to 90%, in good agreement with the capacitances ratio.

It was shown that the high-frequency CPE behaviour observed for the ODA treated sample can be successfully analysed by a power-law resistivity model linked to the resistivity variation in the ODA layer (non-through pores). On the other hand, the low-frequency CPE behaviour was attributed to the double-layer capacitance at the bottom of the pores. The impedance of the through-pores is usually represented by a resistance, R_{pore}, associated to the electrolyte resistance in the porosity. Thus, the equivalent circuit commonly used for organic coatings (Fig. 10), appeared appropriate to describe the electrochemical behaviour of the ODA treated carbon steel [57]. In Fig. 10, the experimental data are in perfect agreement with the fitted data ($\chi^2 = 0.32$).

Similar results (ODA film thickness, permittivity, resistivity profile and inhibitive efficiency) were obtained with another type of steel (100C6 grade) showing that this procedure was reproducible for characterizing thin films behaviour on carbon steel electrodes.

5. Conclusions

In the present study, the physical description of an ODA film formed on a carbon steel surface has been carried out by *ex situ* (optical observations, drop angle measurements and XPS analysis) and *in situ* measurements (electrochemical impedance spectroscopy). From the XPS analysis, the film thickness in dry and vacuum conditions was estimated between 2 and 10 nm. The impedance data were analysed with a power-law model to describe the non-ideal behaviour of the system and to extract quantitative parameters, such as the dielectric film permittivity and the film thickness. All the regressed parameters were in agreement with those graphically estimated. The (*in situ*) film thickness was about 16 nm, in the same order of magnitude than that estimated from (*ex situ*) XPS analysis. The in-depth resistivity profile highlighted a narrow part of high resistivity at the steel/ODA film interface. It was shown that approximately 10% of the carbon steel surface was accessible to the electrolyte, in agreement with an instantaneous inhibitive

efficiency of about 90%.

This work, based on both the use of graphical methods and of the power-law model for impedance data analysis, gave new insights and methodologies for the *in situ* characterization of organic thin films on conductive surfaces.

References

[1] I. Betova, M. Bojinov, T. Saario, Film-forming Amines in Steam/Water Cycles – Structure, Properties, and Influence on Corrosion, VTT. VTT-R-0323, 2014, pp. 1–41.

[2] C.W. Turner, L. Case, Fouling of nuclear steam generators : fundamental studies, operating experience and remedial measures using chemical additives, AECL Nucl. Rev. 2 (2013) 61–88.

[3] Technical Guidance Document: Application of Film-forming Amines in Fossil, Combined Cycle, and Biomass Power Plants, IAPWS, 2016.

[4] W. Hater, D. Olivet, N. Rudschützky, The chemistry and properties of organic boiler feedwater additives based on film-forming amines and their use in steam generators, Powerpl. Chem. 11 (2009) 90–96.

[5] R. Crovetto, A. Rossi, D. Meskers, C. Pierce, J. Melzer, K. Pearson, State of Knowledge on Film-forming Amines 2015, EPRI, Palo Alto, CA, 2015, 2015. 3002003678.

[6] K. Sipilä, T. Saario, Effect of Octadecylamine on Carbon Steel Corrosion under PWR Secondary Side Conditions, VTT, 2014, pp. 1–16.

[7] S. Cao, J. Hu, J. Xie, Q. Liang, L. Yin, Research on the film-forming characteristics of octadecylamine at high temperatures, Anti-corrosion Meth. Mater. 60 (2013) 14–19.

[8] Q.-Q. Liao, G.-D. Zhou, H.-H. Ge, L.-M. Qi, Characterisation of surface film on iron samples treated with octadecylamine, Corrosion Eng. Sci. Technol. 42 (2007) 102–105.

[9] H.-H. Ge, G.-D. Zhou, Q.-Q. Liao, Y.G. Lee, B.H. Loo, A study of anti-corrosion behavior of octadecylamine-treated iron samples, Appl. Surf. Sci. 156 (2000) 39–46.

[10] R. Wagner, E. Czempik, Preservation of boilers and turbines with the surface active substance octadecylamine (ODA), VGB PowerTech J 2014 (2014) 2–5.

[11] E.V. Chernyshev, E.N. Veprov, V.A. Petrov, S.L. Bogdanov, T.Y. Levina, T.I. Petrova, V.I. Kashinskii, A.A. Zonov, A.E. Verkhovskii, Increasing the corrosion resistance of equipment due to the use of film-forming amines, Power Technol. Eng. 40 (2006) 34–37.

[12] A.V. Kurshakov, A.V. Ryzhenkov, A.A. Bodrov, O.V. Ryzhenkov, A.A. Patakin, E.F. Chernov, Heat transfer enhancement in steam-turbine condensers with the use of surface-active substances, Therm. Eng. 61 (2014) 785–789.

[13] F. Mao, C. Dong, D.D. Macdonald, Effect of octadecylamine on the corrosion behavior of Type 316SS in acetate buffer, Corrosion Sci. 98 (2015) 192–200.

[14] B.N. Khodyrev, A.L. Krichevtsov, A.A. Sokolyuk, Studying the processes relating to oxidation of organic substances contained in the coolant of thermal and nuclear power stations, Therm. Eng. 57 (2010) 553–559.

[15] R.F.M. Lobo, M.A. Pereira-Da-Silva, M. Raposo, R.M. Faria, O.N. Oliveira, In situ thickness measurements of ultra-thin multilayer polymer films by atomic force microscopy, Nanotechnology 10 (1999) 389–393.

[16] S. Campen, J.H. Green, G.D. Lamb, H.A. Spikes, *In situ* study of model organic friction modifiers using liquid cell AFM: self-assembly of octadecylamine, Tribol. Lett. 58 (2015).

[17] J. Oviedo, M.A. San-Miguel, J.A. Heredia-Guerrero, J.J. Benítez, Electrostatic induced molecular tilting in self-assembled monolayers of n-octadecylamine on mica, J. Phys. Chem. C 116 (2012) 7099–7105.

[18] K.G. Patil, V. Santhanam, S.K. Biswas, K.G. Ayappa, Combined atomic force microscopy and modeling study of the evolution of octadecylamine films on a mica surface, J. Phys. Chem. C 114 (2010) 3549–3559.

[19] N. Srisuwan, N. Ochoa, N. Pébère, B. Tribollet, Variation of carbon steel corrosion rate with flow conditions in the presence of an inhibitive formulation, Corrosion Sci. 50 (2008) 1245–1250.

[20] W. Kuang, J.A. Mathews, D.D. Macdonald, The effect of Anodamine on the corrosion behavior of 1018 mild steel in deionized water:I. Immersion and polarization tests, Electrochim. Acta 127 (2014) 79–85.

[21] W. Kuang, J.A. Mathews, M.L. Taylor, D.D. Macdonald, The effect of Anodamine on the corrosion behavior of 1018 mild steel in deionized water: II. Electrochemical Impedance Analysis, Electrochim. Acta 136 (2014) 493–503.

[22] H. Otmacic Curkovic, E. Stupnisek-Lisac, H. Takenouti, The influence of pH value on the efficiency of imidazole based corrosion inhibitors of copper, Corrosion Sci. 52 (2010) 398–405.

[23] M. Benoit, C. Bataillon, B. Gwinner, F. Miserque, M.E. Orazem, C.M. Sánchez-sánchez, B. Tribollet, V. Vivier, Comparison of different methods for measuring the passive film thickness on metals, Electrochim. Acta 201 (2016) 340–347.

[24] T. Barrès, B. Tribollet, O. Stephan, H. Montigaud, M. Boinet, Y. Cohin, Characterization of the porosity of silicon nitride thin layers by electrochemical impedance spectroscopy, Electrochim. Acta 227 (2017) 1–6.

[25] S. Chakri, I. Frateur, M.E. Orazem, E.M.M. Sutter, T.T.M. Tran, B. Tribollet, V. Vivier, Improved EIS analysis of the electrochemical behaviour of carbon steel in alkaline solution, Electrochim. Acta 246 (2017) 924–930.

[26] Y. Ben Amor, E. Sutter, H. Takenouti, B. Tribollet, M. Boinet, R. Faure, J. Balencie, G. Durieu, Electrochemical study of the tarnish layer of silver deposited on glass, Electrochim. Acta 131 (2014) 89–95.

[27] S. Mirhashemihaghighi, J. Światowska, V. Maurice, A. Seyeux, S. Zanna, E. Salmi, M. Ritala, P. Marcus, Corrosion protection of aluminium by ultra-thin atomic layer deposited alumina coatings, Corrosion Sci. 106 (2016) 16–24.

[28] M. BenSalah, R. Sabot, E. Triki, L. Dhouibi, P. Refait, M. Jeannin, Passivity of Sanicro28 (UNS N-08028) stainless steel in polluted phosphoric acid at different temperatures studied by electrochemical impedance spectroscopy and Mott-Schottky analysis, Corrosion Sci. 86 (2014) 61–70.

[29] A.T. Tran, F. Huet, K. Ngo, P. Rousseau, Artefacts in electrochemical impedance measurement in electrolytic solutions due to the reference electrode, Electrochim. Acta 56 (2011) 8034–8039.

[30] B.A. Boukamp, A linear Kronig-Kramers transform test for immittance data validation, J. Electrochem. Soc. 142 (1995) 1885.

[31] M. Schönleber, D. Klotz, E. Ivers-Tiffée, A method for improving the robustness of linear Kramers-Kronig validity tests, Electrochim. Acta 131 (2014) 20–27.

[32] Lin-KK tool, (n.d.) http://www.iwe.kit.edu/Lin-KK.php.

[33] M.E. Orazem, N. Pébère, B. Tribollet, Enhanced graphical representation of electrochemical impedance data, J. Electrochem. Soc. 153 (2006) B129–B136.

[34] A.S. Nguyen, N. Causse, M. Musiani, M.E. Orazem, N. Pébère, B. Tribollet, V. Vivier, Determination of water uptake in organic coatings deposited on 2024 aluminium alloy: comparison between impedance measurements and gravimetry, Prog. Org. Coating 112 (2017) 93–100.

[35] B. Hirschorn, M.E. Orazem, B. Tribollet, V. Vivier, I. Frateur, M. Musiani, Constant-Phase-Element behavior caused by resistivity distributions in films. I: Theory, J. Electrochem. Soc. 157 (2010) C452–C457.

[36] B. Hirschorn, M.E. Orazem, B. Tribollet, V. Vivier, I. Frateur, M. Musiani, Constant-Phase-Element behavior caused by resistivity distributions in films. II: Applications, J. Electrochem. Soc. 157 (2010) C458–C463.

[37] T.T.M. Tran, B. Tribollet, E.M.M. Sutter, New insights into the cathodic dissolution of aluminium using electrochemical methods, Electrochim. Acta 216 (2016) 58–67.

[38] D. You, N. Pebere, F. Dabosi, An investigation of the corrosion of pure iron by electrochemical techniques and in situ observations, Corrosion Sci. 34 (1993) 5–15.

[39] J.J. Chen, N. Winograd, The adsorption and decomposition of methylamine on Pd{111}, Surf. Sci. 326 (1995) 285–300.

[40] D.M. Thornburg, R.J. Madix, Cleavage of NH bonds by active oxygen on Ag(110). II. Selective oxidation of ethylamine to acetonitrile, Surf. Sci. 226 (1990) 61–76.

[41] M. Grunze, R.N. Lamb, Adhesion of vapour phase deposited ultra-thin film polymide films on polycrystalline silver, Surf. Sci. 204 (1988) 183–212.

[42] N. Alzate-Carvajal, E.V. Basiuk, V. Meza-Laguna, I. Puente-Lee, M.H. Farías, N. Bogdanchikova, V.A. Basiuk, Solvent-free one-step covalent functionalization of graphene oxide and nanodiamond with amines, RSC Adv. 6 (2016) 113596–113610.

[43] J.J. Benítez, M.A. San-Miguel, S. Domínguez-Meister, J.A. Heredia-Guerrero, M. Salmeron, Structure and chemical state of octadecylamine self-assembled monolayers on mica, J. Phys. Chem. C 115 (2011) 19716–19723.

[44] O. Olivares-Xometl, N.V. Likhanova, R. Martínez-Palou, M.A. Domínguez-Aguilar, Electrochemistry and XPS study of an imidazoline as corrosion inhibitor of mild steel in an acidic environment, Mater. Corros. 60 (2009) 14–21.

[45] A.P. Grosvenor, B.A. Kobe, M.C. Biesinger, N.S. McIntyre, Investigation of multiplet splitting of Fe 2p XPS spectra and bonding in iron compounds, Surf. Interface Anal. 36 (2004) 1564–1574.

[46] T. Yamashita, P. Hayes, Analysis of XPS spectra of Fe2+ and Fe3+ ions in oxide materials, Appl. Surf. Sci. 254 (2008) 2441–2449.

[47] D. Briggs, M.P. Seah, Practical Surface Analysis, second ed., John Wiley & Sons, 1993.

[48] M.A. Rampi, O.J.A. Schueller, G.M. Whitesides, Alkanethiol self-assembled monolayers as the dielectric of capacitors with nanoscale thickness, Appl. Phys. Lett. 72 (1998) 1781–1783.

[49] F.S. Damos, R.C.S. Luz, L.T. Kubota, Determination of thickness, dielectric constant of thiol films, and kinetics of adsorption using surface plasmon resonance, Langmuir 21 (2005) 602–609.

[50] F. Gala, G. Zollo, Dielectric properties of self-assembled monolayer coatings on a (111) silicon substrate, J. Phys. Chem. C 119 (2015) 7264–7274.

[51] J.J. Benitez, O.R. De La Fuente, I. Díez-Pérez, F. Sanz, M. Salmeron, Dielectric properties of self-assembled layers of octadecylamine on mica in dry and humid environments, J. Chem. Phys. 123 (2005) 1–6.

[52] C.E.D. Chidsey, D.N. Loiacono, Chemical functionality in self-assembled monolayers: structural and electrochemical Properties, Langmuir 6 (1990) 682–691.

[53] D.R. Lide, CRC Handbook of Chemistry and Physics, 84th edition, 2003.

[54] Y. Ben Amor, E.M.M. Sutter, H. Takenouti, M.E. Orazem, B. Tribollet, Interpretation of electrochemical impedance for corrosion of a coated silver film in terms of a pore-in-pore model, J. Electrochem. Soc. 161 (2014) 573–579.

[55] G.J. Brug, A.L.G. van den Eeden, M. Sluyters-Rehbach, J.H. Sluyters, The analysis of electrode impedances complicated by the presence of a constant phase element, J. Electroanal. Chem. 176 (1984) 275–295.

[56] B. Hirschorn, M.E. Orazem, B. Tribollet, V. Vivier, I. Frateur, M. Musiani, Determination of effective capacitance and film thickness from constant-phase-element parameters, Electrochim. Acta 55 (2010) 6218–6227.

[57] L. Beaunier, I. Epelboin, J.C. Lestrade, H. Takenouti, Etude electrochimique, et par microscopie electronique a balayage, du fer recouvert de peinture, Surf. Technol. 4 (1976) 237–254.